Three-dimension simulation of two-phase flows in a thin gas flow channel of PEM fuel cell using a volume of fluid method

Jingtian Wu [a], Yiming Li [b],[**], Yun Wang [a],[*]

[a] *Renewable Energy Resources Lab (RERL), Department of Mechanical and Aerospace Engineering, University of California, Irvine, CA, 92697-3975, United States*
[b] *China University of Petroleum, Beijing, 102249, China*

HIGHLIGHTS

- 3D VOF simulation of two-phase flow in a thin gas flow channel is carried out.
- Stable film flow is predicted for the various contact angles of channel walls.
- Contact angle is shown to affect the interfacial curvature of the two-phase flow.
- Contact angle is shown to have small impact on the gas pressure drop.
- Prediction of P_g and liquid fraction agrees with experimental/theoretical results.

ARTICLE INFO

ABSTRACT

This study investigates the two-phase flow in a thin gas flow channel of PEM fuel cells and wall contact angle's impact using the volume of fluid (VOF) method with tracked two-phase interface. The VOF results are compared with experimental data, theoretical solution and analytical data in terms of flow pattern, pressure drop and water fraction. Stable film flow is predicted, as observed experimentally, for the contact angle ranging from 5° to 40° including varying contact angles at different walls of a channel. The contact angle is found to have small impact on the gas pressure drop for the stratified flow regime, but it determines the meniscus of the two-phase interface, which affects the optical detection of the liquid thickness in experiment. The work is important to study of two-phase flow dynamics, multichannel design, experimental design and control of two-phase flows in thin gas flow channels for PEM fuel cells.

Published by Elsevier Ltd on behalf of Hydrogen Energy Publications LLC.

Introduction

Micro-channel plays an important role in the application of engineering, such as micro heat exchangers, PEM fuel cells and microfluidics. In PEM fuel cells, gas flow channels are important components with a cross-section dimension around 1 mm and a length around 10 cm, which supply hydrogen and oxygen gases for electrochemical reactions [1]. Two-phase flow is frequently encountered in the gas flow channels due to water production by fuel cells, and

---

significantly influences fuel cell operation. For example, blockage of a microchannel by liquid water will terminate the hydrogen/oxygen supply to local reaction site. The flow pattern influences the pressure drop and hence the gas flow rates in gas flow channels. Further, it has been observed water accumulation and dynamics occur near the channel-manifold connection, which increases difficulties in two-phase flow control.

Many works have been attempted to understand the complex two-phase flow in mini/micro channels, including flow patterns, two-phase pressure drop, and phase volume fraction. Ghiaasiaan [2,3] experimentally investigated the gas-liquid two-phase flow patterns, void fraction and pressure drop in horizontal microchannels with circular and triangular cross-sections at a variety of superficial gas and liquid velocities. Kawaji [4] studied the channel diameter's impact on two-phase flow, indicating that flow patterns in the channels of a diameter less than 100 μm is different from that in mini-channels due to viscous and surface tension effects. Serizawa [5] studied the flow patterns in circular tubes of 20, 25 and 100 μm and for steam–water flow in a 50 μm circular tube at a broad range of superficial air and water velocities. He concluded that two-phase flow patterns are sensitive to the surface conditions of the inner wall of the test tube. Cubaud [6] experimentally investigated the two-phase flow in microchannels with surface modifications and found that reduction in the channel size dramatically enhances the wall's effects on two-phase flows. Adroher and Wang [9] investigated the patterns of air-liquid water two-phase flows in a regular microchannel of PEM fuel cell, indicative of the occurrence of wavy, annulus, wavy-annulus and slug-annular regimes. Similar flow patterns were also observed by others [7,8].

Modeling is important to two-phase flow study. Several types of two-phase models have been proposed for channel flows, including homogeneous models, separated flow models, and other physics-based formulation. For homogeneous flow models, two-phase flows are treated as a single-phase flow by using average quantities as major variables regardless of flow patterns. https://www.sciencedirect.com/science/article/pii/S0017931013009563 [10,11] Various empirical correlations using the Lockhart-Martinelli parameter, following the Martinelli method https://www.sciencedirect.com/science/article/pii/S0017931013009563 [12], have also been proposed to investigate two-phase flow and validate experimental data https://www.sciencedirect.com/science/article/pii/S0017931013009563 [13–17]. In micro-/mini-channels, the channel space can be treated as a straight regular pore structure, thus Darcy's law applies for each phase. Two-fluid models, consisting of two sets of flow equations to describe individual phase flow, have been developed with the phase interaction described by the relative permeabilities https://www.sciencedirect.com/science/article/pii/S0017931013009563 [18–22]. Fan [23] carried out both experiment and Lattice Boltzmann simulation to study two-phase flow in microchannels. They found flow regimes depend on the capillary number and bubble breakup is induced by the phase pressure difference. Mehdizadeh [24] simulated slug flows in microchannels with constant heat flux using Volume of Fluid (VOF) method and found that short slugs could

significantly improve the heat transfer coefficient. Qian [25] simulated the Taylor slug flow in microchannel with varying cross-sections and concluded that the gas slug length increases with increasing superficial gas velocity and decreasing superficial liquid velocity. Fang [26] employed VOF methods to simulate the vapor-venting process in a rectangular microchannel and found that it effectively mitigates vapor accumulation by reducing pressure drop and suppressing local dry-out. In PEM fuel cells, Wang [18] developed a two-fluid model to evaluate and analyze the two-phase flow in a novel porous-media flow field for PEM fuel cells. Darcy's law was applied to both air and liquid phases. One dimensional (1-D) analysis gave the two-phase pressure and liquid volume fraction as a function of a number of parameters. The model was validated against previous models and experimental data for hydrophilic micro channels [27,28], mixed-wettability thin channels [29], and mixed wettability channel with a rough surface [30].

Though experimental and numerical studies have been attempted, two-phase flow in microchannels is complex, requiring additional efforts to understand and predict. For example, the contact angle's impacts will be both scientifically and technologically interesting and valuable for two-phase flow control. Recently, two-phase flow in thin channels has attracted research attention for PEM fuel cells. The Toyota Mirai vehicles adopt an about 0.3 mm thick flow field for their fuel cell stack. The experimental study by Lewis and Wang [28] indicated that the two-phase flow in a thin gas flow channel remains in the stratified pattern for a wide range of fuel cell operations. This kind of single flow pattern is desirable in the fuel cell application, which mitigates occurrence of flow maldistribution and improves pressure prediction and reactant supply. This study employed the VOF method, capable of tracking the two-phase interface, to investigate the air-liquid flow in a thin gas flow microchannel, including the two-phase pressure drop, liquid volume fraction and contact angle's impacts. To directly compare with the experimental study [28], this work is focused on the stratified flow pattern and the experimental operating condition to bring insights in view of modeling on the two-phase flow in thin gas flow channels. We considered the contact angle ranging from 5° to 40°, in which the VOF predicts stable water film formation, as observed experimentally. For the contact angle over 40°, the VOF may predict unstable flows, which will be investigated in a separate study. The numerical results were also compared with a variety of other model predictions.

Volume of fluid (VOF) model

Fig. 1(a) shows the flow field of a PEM fuel cell, which consists of several serpentine channels arranged in parallel. In the cathode of PEM fuel cell, the oxygen reduction reaction (ORR): $4H^+ + 4e^- + O2 \rightarrow 2H_2O$ takes place with water as the only byproduct. Two-phase flow is originated from the ORR water production, as shown in Fig. 1(b), consisting of liquid water and air flows. Fig. 1(c) shows stratified two-phase flow observed in a thin channel. A VOF method is adopted to describe the individual flows with the interface of the two phases tracked by using the phase volume fraction.

Governing equations

The governing equations for the two-phase VOF model in this study consist of three conservation equations [37]:

Continuity equation:

$$\nabla \cdot u = 0 \tag{1}$$

where u denotes the liquid/gas velocity. Its discretization is given by:

$$\sum_f \varphi_f = 0 \tag{1.1}$$

where φ_f is the volume flux across the surface of individual grid.

Phase conservation equation:

$$\frac{\partial C}{\partial t} + \nabla \cdot (uC) + \nabla \cdot [(1 - C)Cu_r] = 0 \tag{2}$$

where u denotes liquid/gas velcocity, C is volume fraction of liquid phase and u_r is relative velocity between liquid and gas. Its discretization is given by:

$$\frac{C^{n+1} - C^n}{\Delta t} = -\frac{1}{\Delta V} \sum_f (F_u + \lambda F_s)^n \tag{2.1}$$

where the left term uses the Forward Euler Scheme with Δt the time step; ΔV denotes the volume of computational grid, and f denotes the surface of a computational cell. λ is 1 at the interface and 0 elsewhere. $F_u = \varphi_f C_f$ and $F_s = \varphi_f C_f + \varphi_{rf} C_{rf} (1 - C)_{rf} - F_u$, where φ_f and φ_{rf} denote volume fluxes across the surface and interface, respectively.

Momentum equation:

$$\frac{\partial \rho u}{\partial t} + \nabla \cdot (\rho uu) = -\nabla p + \mu \nabla^2 u + \sigma \kappa \nabla C \tag{3}$$

where ρ denotes density of gas/liquid, p is thermodynamic pressure, μ is dynamic viscosity of gas/liquid, σ is surface tension at gas/liquid interface and κ is the mean curvature of the phase interface. Its discretization is given by:

$$\frac{\rho^{n+1} u_p - (\rho u)^n}{\Delta t} \Delta V + \sum_f (\rho_f \varphi_f)^n u_f = \sum_f \mu_f^{n+1} \left(\nabla_f^\perp u \right) \Delta S \tag{3.1}$$

where u_p is the predicted velocity and $\nabla_f^\perp$ the surface gradient operator acting on u.

The physical properties of the two-phase mixture are determined by the water and air properties using their corresponding volume fractions as the weights:

$$\rho = \rho_w C + \rho_a (1 - C) \tag{4}$$

$$\mu = \mu_w \mu + \mu_a (1 - C) \tag{5}$$

where ρ_w and ρ_a are densities of water and air, respectively, μ_w and μ_a are dynamic viscosity of water and air.

The effective velocity u and relative velocity u_r are given by:

$$u = Cu_w + (1 - C)u_a \tag{6}$$

$$u_r = u_w - u_a \tag{7}$$

The continuity equation for incompressible flow applies for the air flow because it is under low velocity and thus the air density can be assumed constant. In the phase conservation equation [33], the phase fraction C takes the value of 0 or 1 if the cell is full of air or water, respectively. A value of C between 0 and 1 indicates that the cell contains an air-liquid interface. To account for the effect of surface tension at the gas-liquid interface, the continuum surface force(CSF) model [31] is adopted to add a force source $f = \sigma \kappa \nabla C$ to the momentum equation, where σ is the surface tension and κ is the mean curvature of the phase interface given by

$$-\nabla \cdot n = -\nabla \left(\frac{\nabla C}{|\nabla C|} \right).$$

When the interface contacts a solid wall of a given contact angle θ, the surface unit normal n is determined by the following equation:

$$n = n_w \cos \theta + t_w \sin \theta \tag{8}$$

where n_w is the unit vector normal to the wall and t_w is the unit vector tangential to the wall. In this study, the contact angle θ is changed to investigate its impacts on two-phase flow pattern, pressure drop, and interface shape. In addition, channel flows with two walls set at different contact angles are also investigated.
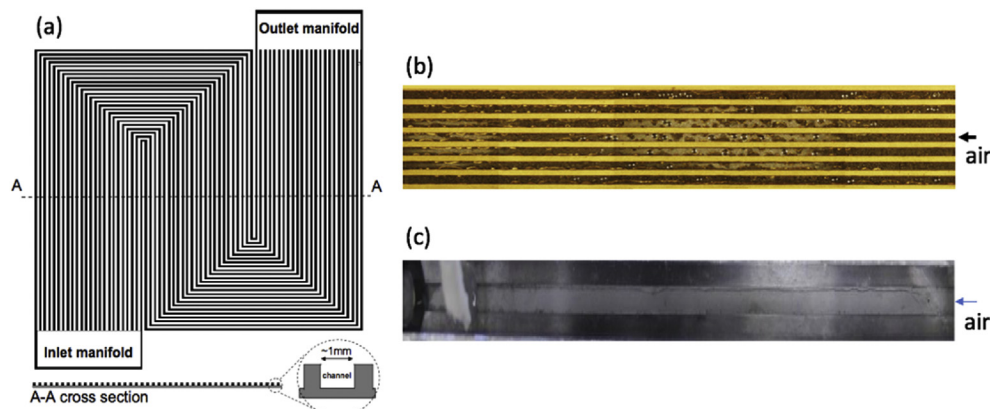

Fig. 1 — (a) A serpentine flow field of a 200 cm^2 PEM fuel cell; and optical visualization of: (b) two-phase flow in regular gas flow channels and (c) stratified flow observed in a thin gas flow channel [7,28].

Initial and boundary conditions

The channel has a dimension of 164 mm by 3 mm by 0.3 mm (L × w × h). For the air or water inlet, an air or water velocity is set according to experimental conditions. For flow outlet, the gradients of velocity and pressure along the channel direction are set to zero. The no-slip boundaries are imposed on the solid walls, where a contact angle θ is set as well. For no-slip boundary condition, both gas and liquid velocities are set zero at the wall surface. Initially, there is no liquid water in the channel.

Numerical procedures

The micro-channel, computational flow field, was discretized with a total of 100,000 hexahedral meshes and fine grids used close to the wall, as shown in Fig. 2. Mesh independent study was carried out, showing the selected computational domain is adequate to capture the two-phase flow. The open source software Open FOAM was adopted to perform the numerical simulations and PIMPLE algorithm scheme, which combines the pressure-implicit split-operator (PISO) and the semi-implicit method for pressure-linked equations (SIMPLE) algorithm, was used for the coupling solution of the pressure and velocity. The open-MPI was adopted for parallel computation. The time step was set 1×10^{-6} s. Each case took about one week by using 28 Intel Xeon @2.93 GHz processors in parallel. All the physical and model parameters are listed in Table 1.

Results and discussion

Fig. 3 compares the air-liquid interface along the channel at the superficial air velocity 1.69 m/s and water velocity 0.01 m/s. It is seen that a film is predicted as also observed experimentally. The predicted thickness agrees with the experimentally determined water thickness, except near the water injection port which is set at the middle of the channel in experiment, as shown in Fig. 4. The water film remains an
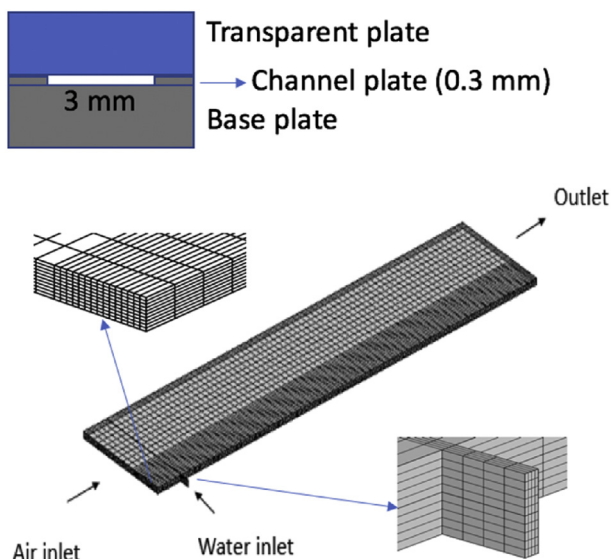

Fig. 2 – Computational domain of a thin gas flow channel.

Table 1 – Physical properties and model parameters.

Name	Symbol	Value
Air density	ρ_g	1.19 $kg\ m^{-3}$
Liquid density	ρ_l	998$kg\ m^{-3}$
Air kinematic viscosity	v_g	$1.55 \times 10^{-5} m^2 s^{-1}$
Liquid kinematic viscosity	v_l	$1 \times 10^{-6} m^2 s^{-1}$
Channel dimension	—	164mm × 3mm × 0.3mm
Contact angle	θ	$5°, 10°, 20°, 30°, 40°$
Surface tension coefficient	σ	7.2×10^{-2} N m^{-1}
Superficial air velocity	v_g	$1.69 \sim 5.08$ m s^{-1}
Superficial liquid velocity	v_l	$5 \times 10^{-5} \sim 1 \times 10^{-2}$ m s^{-1}
Temperature	T	$20°C$
Ambient pressure	P_0	1 atm
Time step in VOF	—	1×10^{-6} s

almost constant thickness along the channel due to no water addition or evaporation after the water injection port, and the two-phase flow remains steady possibly due to the thin channel flow where the channel wall greatly influences the flows and the two-phase interaction occurs only at the very small phase interfacial area. Because of the large impact from the wall, experimental water film shows irregular pattern in local possibly due to roughness or impurity at the wall, which is not taken into account in the VOF simulation. Furthermore, experimental uncertainty, to be shown in Fig. 5, may also contribute to the discrepancy between the VOF prediction and experimental data.

Fig. 5 compares the predicted thickness of liquid water film with experimental work, other model data and analytical result. It shows that the data agree reasonably well: as the flow rate ratio increases, the liquid thickness decreases rapidly. The analytical result of Wang's model [18] is based on the exponential of the relative permeability n_k of 1.159 and refers to the liquid saturation or volume fraction in the channel. Note that the residual liquid is assumed to be zero in the simulation and analytical solutions, which may occur in experiment. In addition, in all the simulated cases film flows formed, as observed experimentally, thus the film thickness can be directly measured through the two-phase interface. To compare with the experimental optical measurement, the thickness was evaluated by the liquid line at the transparent plate.

Fig. 6 presents the two-phase interfaces at three contact angles, i.e. 5°, 10° and 30°. Due to symmetry, half of the channel is simulated with the bottom surface as the symmetry plane. First, it can be seen that the upper wall's contact angle changes the water-air interface in the local due to the difference in wall attraction for the three cases. The interface at the upper wall is around the specified contact angle, which is primarily due to the dominant surface tension in comparison with the forces imposed by flow and gravity, as indicated by a few dimensionless numbers for the water velocity (V) of 0.01 m/s: the Bond number $Bo = \frac{\Delta \rho g L^2}{\sigma} \sim 1.0 \times 10^{-2}$, the Capillary number: $Ca = \frac{\mu V}{\sigma} \sim 1.0 \times 10^{-4}$, and the Weber number: $We = \frac{\rho V^2 L}{\sigma} \sim 1.0 \times 10^{-3}$, where $\Delta \rho$ is the density difference, σ the surface tension coefficient, g the gravitational acceleration, L the characteristic length, ρ the water density and μ the dynamic viscosity of water. In addition, it is evident that the liquid water at the transparent plate is drawn up due to the hydrophilic wall. In the optical observation through the transparent
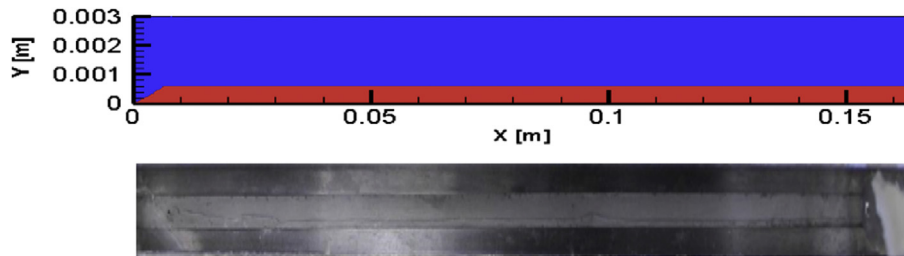
Fig. 3 − VOF predicted liquid water location at the transparent plate, in comparison with the experimental image of water film formation [28], at the superficial air velocity of 1.69 m/s, 30° wall contact angle, and water velocity of 0.01 m/s.
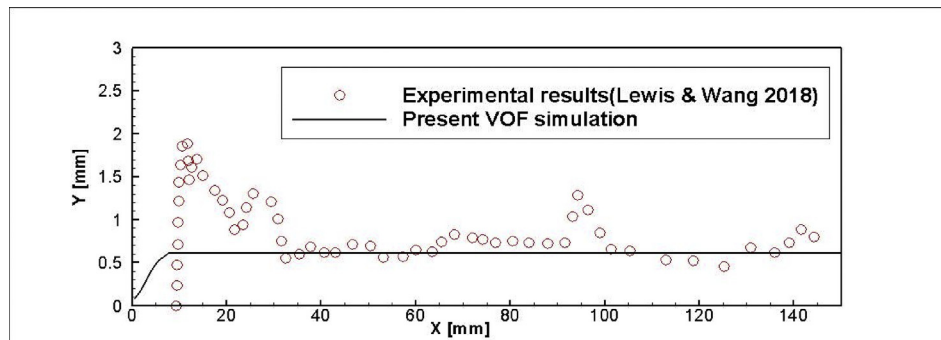

Fig. 4 − Comparison of the predicted water-air interface and experimental data at the superficial air velocity of 1.69 m/s, 30° wall contact angle, and water velocity of 0.01 m/s.

plate, the water line at the transparent plate was captured as the water thickness of the channel flow, which raises uncertainty in the thickness determination due to the meniscus formation. The uncertainty in film thickness determination using the optical method is small due to the thin thickness of the channel, but could be large for a very small contact angle.
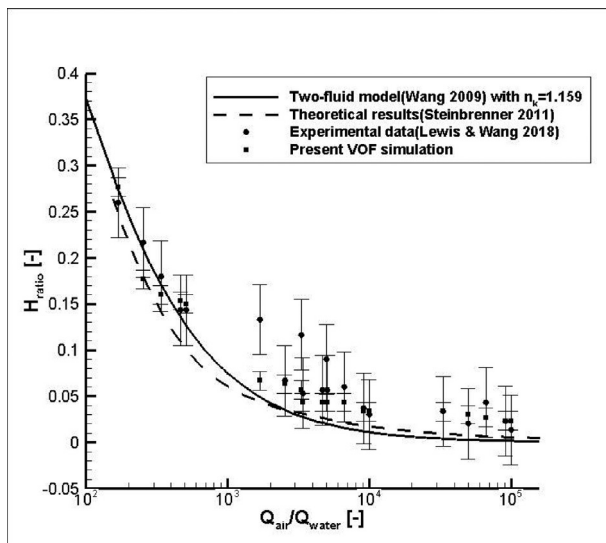

Fig. 5 − Comparison of VOF predicted water thickness using 30° wall contact angle and experimental, theoretical [32], and other model data.

For a completely wetting surface, liquid water spreading over the surface makes it difficult to determine the film thickness. In addition, to facilitate optical detection one channel wall will be replaced by a transparent plate, allowing a direct observation of the two-phase flow. The transparent plate usually has a contact angle different with the base plate. Fig. 6 (right) presents the impacts of varying contact angle walls on the interface morphology, showing that the contact angles of both the upper and lower planes affect the shape of the two-phase interface.

Due to liquid presence, the channel gas flow space narrows down, leading to a raised pressure drop. Fig. 7 presents the two-phase pressure drop along the channel versus single phase one. It is seen an almost linear drop for both single- and two-phase flows with the two-phase pressure drop larger than the single-phase one. In addition, the pressure contour indicates the pressure varies little in the direction perpendicular to the along-channel direction, similar to that of the single-phase channel flow.

Figs. 8 and 9 compare the predicted two-phase pressure drop with experimental data and predictions from the homogeneous, separated, and two-fluid models. It is seen that the VOF prediction agrees well with these data. Effects of the contact angle on the pressure drop are also presented, which is negligible as long as the two-phase flow remains as a steady stratified flow. For a contact angle above 40°, the VOF prediction shows unstable flows in certain cases. At this stage, it is unclear the observed unstable flows are due to the VOF numerical scheme, selection of the time step, physical
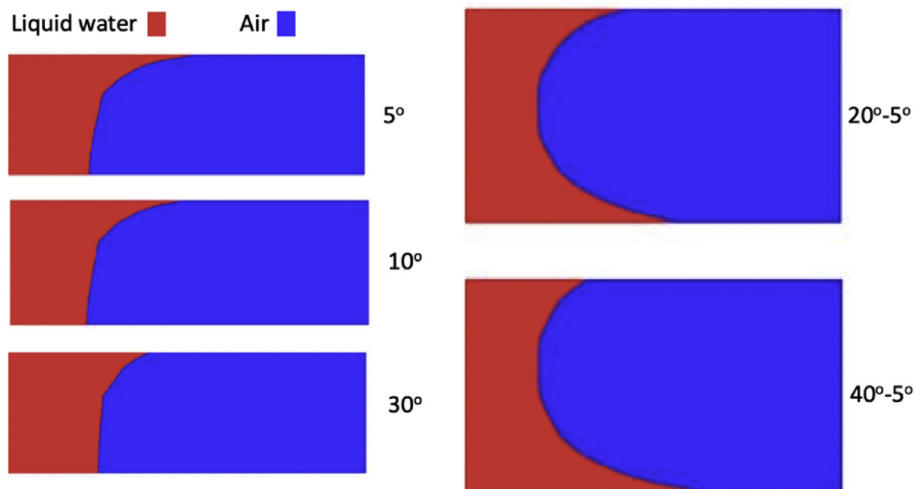
Fig. 6 – Predicted two-phase interface at a cross section of the channel for three contact angles (left) and two varying contact angle (right). For the left plots, the lower plane is set symmetry. For the right plot, the above plane has a 20° or 40° contact angle while the rest are set at 5°. The red denotes the liquid water phase and blue represents the air phase. (For interpretation of the references to color in this figure legend, the reader is referred to the Web version of this article.)
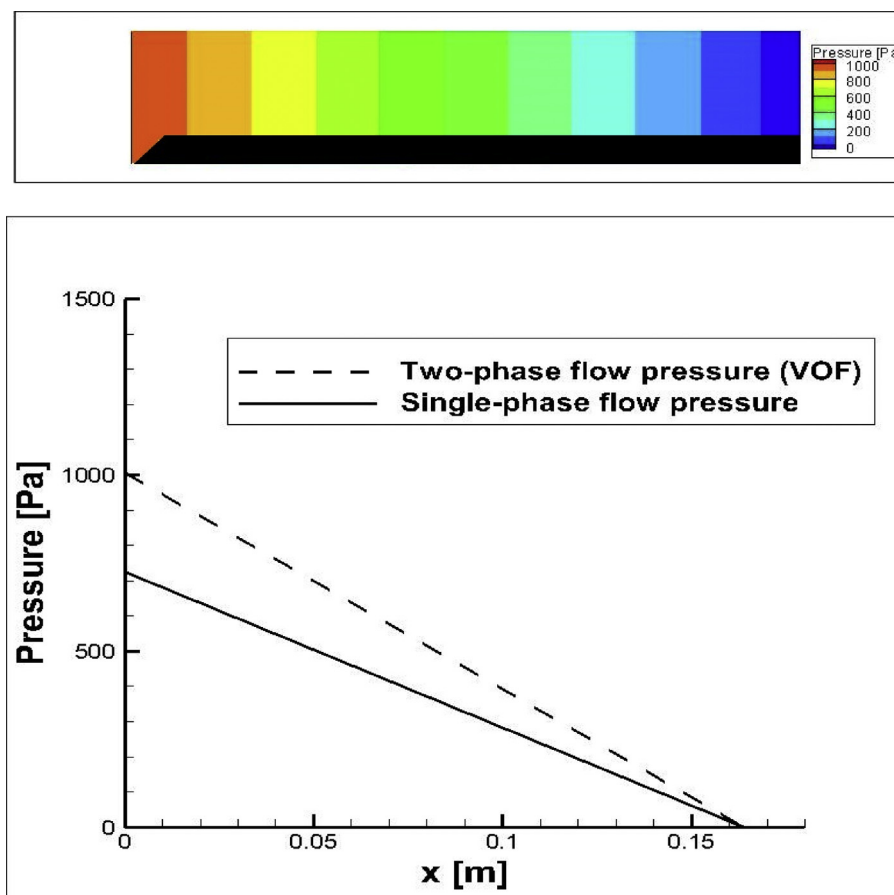

Fig. 7 – Predicted gas pressure contours at 30° wall contact angle (above); and pressure drop along the channel (below) at the superficial air velocity of 1.69 m/s and liquid velocity of 0.01 m/s in comparison with the single-phase pressure at the superficial air velocity of 1.69 m/s.
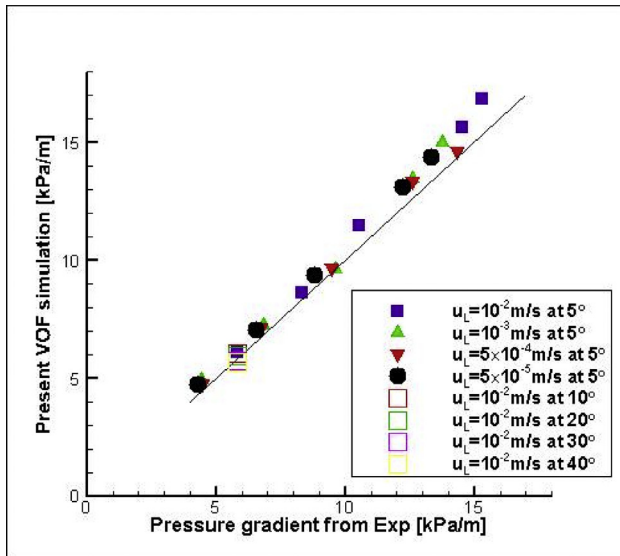
Fig. 8 − Predicted pressure drop using various contact angles, in comparison with experimental data [28].

Fig. 10 − Predicted pressure drop in a channel of varying contact angle walls in comparison with experimental data [28]. The two-phase interfaces are plotted in Fig. 6.

phenomena, or droplet attachment (residual liquid) at the wall surface [34]. The causes to instability under a contact angle over 40° are under further investigation. In addition, it is desirable to have a stable film flow pattern in the gas flow channels of PEM fuel cells [1] because the stable two-phase flow pattern will improve pressure prediction, reduce reactant gas transport resistance to the reaction sites, and mitigate flow maldistribution among channels caused by flow pattern shift or flow instability. Fig. 10 presents the comparison of the varying-contact-angle channels with experimental data. Again, the contact angle has negligible impact on the air pressure drop in the range of the selected contact angles, despite the distinct interface shape as disclosed by Fig. 6.
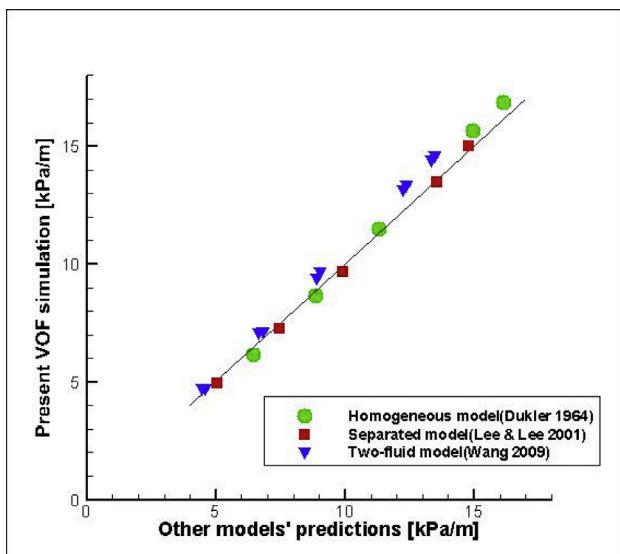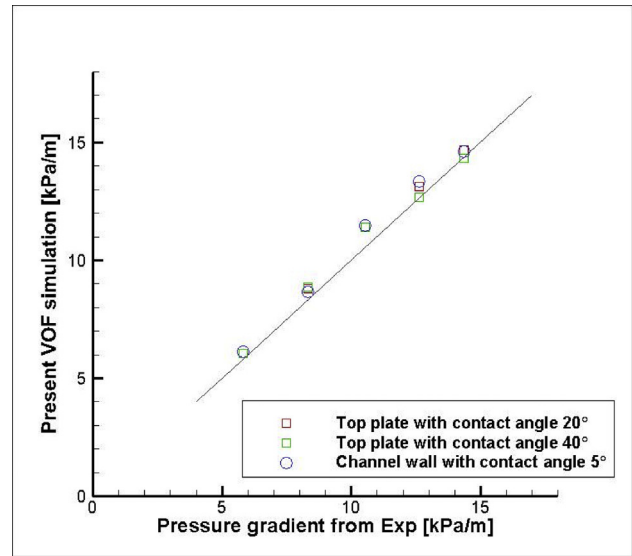
Conclusion

In this study, the 3D VOF method was employed to investigate the two-phase flow dynamics in a thin gas flow channel of PEM fuel cell with a cross-sectional dimension of 3 mm × 0.3 mm. Various contact angles of the channel walls were studied to investigate their impacts on the two-phase interface, film thickness, and the pressure drop. The results were compared with various empirical models, two-fluid model, theoretical solution and experimental results, in terms of the pressure drop and water volume fraction. We found that 1.) the contact angle affects the two-phase flow interface in the thin channel by altering its curvature near the wall. The near-wall's two-phase interface shows an angle close to the wall's contact angle due to the dominant force of surface tension and wall impact. 2.) the VOF prediction indicated that the contact angle may affect the optical observation of the liquid water thickness due to the interface curvature, which raises uncertainty in the experimental method of film thickness determination. 3.) The predicted flow remains in the stratified regime, as experimentally observed, for the contact angle ranging from 5° to 40°. The water fraction agreed well with the two-fluid model, analytical results, and experimental data. 4.) The predicted gas pressure agreed with the experimental data, two-fluid model, theoretical solution and some empirical models. The contact angle showed a negligible impact on the predicted pressure drop in the range of 5° to 40° including varying contact angle walls of a channel, in which the VOF predicted stable water film formation. For the contact angle over 40°, the VOF predicted unstable flows. The film instability is under further investigation for future publication. The validated VOF method can be applied to study two-phase flow in multi-channels, channel-manifold interface, and U-turns in thin gas flow

Fig. 9 − Predicted pressure drop of the wall contact angle at 40° in comparison with various model results [35,36].

channels and other components of PEM fuel cells including GDLs and MPLs.

Acknowledgement

R E F E R E N C E S

[1] Wang Y, Chen KS, Mishler J, Cho SC, Adroher XC. A review of polymer electrolyte membrane fuel cells: technology, applications and needs on fundamental research. Appl Energy 2011;88:981—1007.

[2] Triplett KA, Ghiaasiaan SM. Gas-liquid two-phase flow in microchannels Part I: two-phase flow patterns. Int J Multiph Flow 1999;25:377—94.

[3] Triplett KA, Ghiaasiaan SM. Gas—liquid two-phase flow in microchannels: Part II: void fraction and pressure drop. Int J Multiph Flow 1999;25:395—410.

[4] Chung PM-Y, Kawaji M. The effect of channel diameter on adiabatic two-phase flow characteristics in microchannels. Int J Multiph Flow 2004;30:735—61.

[5] Serizawa A, Feng ZP, Kawara Z. Two-phase flow in microchannels. Exp Therm Fluid Sci 2002;26:703—14.

[6] Cubaud T, Ulmanella U, Ho C. Two-phase flow in microchannels with surface modifications. Fluid Dyn Res 2006;38:772—86.

[7] Wang Y, D.F.R. Diaz, K.S. Chen, Z. Wang, X.C. Adroher. Materials, technological status, and fundamentals of PEM fuel cells—a review. Mater Today 2019. https://doi.org/10.1016/j.mattod.2019.06.005. In press.

[8] Hussaini IS, Wang CY. Visualization and quantification of cathode channel flooding in PEM fuel cells. J Power Sources 2009;187:444—51.

[9] Adroher XC, Wang Y. Ex-situ and modeling study of two-phase flow in a single channel of polymer electrolyte membrane fuel cells. J Power Sources 2011;196:9544—51.

[10] McAdams WH, Woods WK, Heroman LC. Vaporization inside horizontal tubes II-benzene-oil mixtures. Trans ASME 1942;64:193—200.

[11] Cicchitti A, Lombardi C, Silvestri M, Soldaini G, Zavalluilli R. Two-phase cooling experiments pressure drop, heat transfer and burnout measurements. Energy Nucl 1960;7:407—25.

[12] Lockhart RW, Martinelli RC. Proposed correlation of data for isothermal two phase flow, two component flow in pipes. Chem Eng Prog 1949;45:39—48.

[13] Mishima K, Hibiki T. Some characteristics of air-water two-phase flow in small diameter vertical tubes. Int J Multiph Flow 1996;22:703—12.

[14] Sun L, Mishima K. Evaluation analysis of prediction methods for two-phase flow pressure drop in mini-channels. Int J Multiph Flow 2009;35:47—54.

[15] Li W, Wu Z. A general correlation for adiabatic two-phase pressure drop in micro/mini-channels. Int J Heat Mass Transf 2010;53:2732—9.

[16] Zhang W, Hibiki T, Mishima K. Correlations of two-phase frictional pressure drop and void fraction in mini-channel. Int J Heat Mass Transf 2010;53:453—65.

[17] Kim SM, Mudawar I. Universal approach to predicting two-phase frictional pressure drop for adiabatic and condensing mini/micro-channel flows. Int J Heat Mass Transf 2012;55:3246—61.

[18] Wang Y. Porous-media flow fields for polymer electrolyte fuel cells II. Analysis of channel two-phase flow. J Electrochem Soc 2009;156:B1134—41.

[19] Nowamooz A, Radilla G, Fourar M. Non-Darcian two-phase flow in a transparent replica of a rough-walled rock fracture. Water Resour Res 2009;45. W07406.

[20] Fourar M, Lenormand R. A viscous coupling model for relative permeabilities in fractures, Paper SPE 49006. In: SPE annual technical conference and exhibition, New Orleans, LA; 1998.

[21] Huang H, Li Z, Liu S, Lu XY. Shan and chen type multiphase lattice Boltzmann study of viscous coupling effects for two-phase flow in porous media. Int J Numer Methods Fluids 2009;61:341—54.

[22] Chen CY, Horne RN, Fourar M. Experimental study of liquid-gas flow structure effects on relative permeabilities in a fracture. Water Resour Res 2004;40. W08301.

[23] Yu Z, Hemminger O, Fan L. Experiment and lattice Boltzmann simulation of two-phase gas—liquid flows in microchannels. Chem Eng Sci 2007;62:7172—83.

[24] Mehdizadeh A, Sherif SA, Lear WE. Numerical simulation of thermofluid characteristics of two-phase slug flow in microchannels. Int J Heat Mass Transf 2011;54:3457—65.

[25] Qian DY, Lawal A. Numerical study on gas and liquid slugs for Taylor flow in a T-junction microchannel. Chem Eng Sci 2006;61:7609—25.

[26] Fang C, David M, Rogacs A, Goodson K. Volume of fluid simulation of boiling two-phase flow in a vapor-venting microchannel. Frontiers in Heat and Mass Transfer (FHMT) 2010;1. 013002.

[27] Cho SC, Wang Y. Two-phase flow dynamics in a micro hydrophilic channel: a theoretical and experimental study. Int J Heat Mass Transf 2014;70:340—52.

[28] Lewis JM, Wang Y. Two-phase frictional pressure drop and water film thickness in a thin hydrophilic microchannel. Int J Heat Mass Transf 2018;127:813—28.

[29] Lewis JM, Wang Y. Two-phase frictional pressure drop in a thin mixed-wettability microchannel. Int J Heat Mass Transf 2019;128:649—67.

[30] Cho SC, Wang Y. Two-phase flow dynamics in a micro channel with heterogeneous surfaces. Int J Heat Mass Transf 2014;71:349—60.

[31] Brackbill JU, Kothe DB, Zemach C. A continuum method for modeling surface tension. J Comput Phys 1992;100:335—54.

[32] Steinbrenner JE. Two-phase flow phenomena. In: Fuel cell microchannels. Stanford University; 2011.

[33] Hirt CW, Nichols BD. Volume of fluid (VOF) method for the dynamics of free boundaries. J Comput Phys 1981;39:201—25.

[34] Cho SC, Wang Y, Chen KS. Droplet dynamics in a polymer electrolyte fuel cell gas flow channel: forces, deformation, and detachment. I: theoretical and numerical analyses. J Power Sources 2012;206:119—28.

[35] Dukler A, Wicks III M, Cleveland R. Fictional pressure drop in two-phase flow: B. An approach through similarity analysis. A.I.Ch.E J 1964;10:44—51.

[36] Lee HJ, Lee SY. Pressure drop correlations for two-phase flow within horizontal rectangular channels with small heights. Int J Multiph Flow 2001;27:783—96.

[37] Niu ZQ, Wang Y, Jiao K, Wu JT. Two-phase flow dynamics in the gas diffusion layer of proton exchange membrane fuel cells: volume of fluid modeling and comparison with experiment. J Electrochem Soc 2018;165:F613—20.